International Journal of Electronic and Electrical Engineering.
ISSN 0974-2174 Volume 5, Number 2 (2012), pp. 91-111

http://www.irphouse.com

A Spectral based Approach to Power Flow Controlling and Quality Monitoring in IEEE Electrical Bus System

[1]Uppari Srinivasulu, [2]Dr. Sirobhusana Kesavan and [3]B.V. Sanker Ram

[1]Associate Professor, VCE, Dept of EEE,
Shamsabad, Hyderabad, India
E-mail: usrinuphd@gmail.com
[2]Professor & Dept. of EEE, SVIT, Hyderabad, India
E-mail: sirobhusana__k@in.com
[3]Professor, Dept of EEE, JNTU College of Engineering, Hyderabad, India
E-mail: bvsram4321@yahoo.com

Abstract

The effect of very minor variations and their analysis using frequency domain tool is presented in this paper. The disturbances in distributed system is processed in frequency domain to evaluate the variations in magnitude and frequency based and is processed with a advanced learning approach based radial neural network to improve the power quality performance in Distributed power system. For the evaluation of the proposed approach an analysis on IEEE-30 bus system is carried out. The performances were evaluated for the power quality measures to achieve better performance.

Keywords: Power Flow controller, Adaptive learning scheme, Radial Neural network, spectral analysis, 30-Bus system.

Introduction

With the rapid increase in power demands and their compensation, various networks were upcoming in recent past. With the increase in the network layout and its load at the demand side the power flow in power system is getting affected. To compensate the power quality metric in distributed system FACTs devices are developed. Among all FACTs devices unified power flow controller (UPFC) is a dominantly used controller. The UPFC is capable of both supplying and absorbing real and reactive

power and consists of two AC/DC converters. One of the two converters is connected in series with the transmission line through a series transformer and the other in parallel with the line through a shunt transformer. The DC side of the two converters is connected through a common capacitor that provides DC voltage for the converter operation. The power balance between the series and shunt converters is a prerequisite to maintain a constant voltage across the DC capacitor. As the series branch of the UPFC injects a voltage of variable magnitude and phase angle it can exchange real power with the transmission line and thus improves the power flow capability of the line as well as its transient stability limit. The shunt converter exchanges a current of controllable magnitude and power factor angle with the power system. It is normally controlled to balance the real power absorbed from or injected to the power system by the series converter plus the losses by regulating the DC bus voltage at a desired value. Various control strategies to control the series voltage magnitude and angle and the shunt current magnitude have been presented in the references [1]–[4]. The series converter voltage phasor can be decomposed into in-phase and quadrature components with respect to the transmission line current. The in-phase and the quadrature-voltage components are more readily related to the reactive and real power flows in the transmission system. During short-circuit and transient conditions, the decrease in real power can be stopped by controlling the quadrature component of the series converter voltage and hence the improvement in transient stability. The series voltage in phase component is either controlled by the reactive power flow deviation or voltage deviation at the injected bus where the UPFC is located. The transmission line current could be decomposed into in phase and quadrature phase components by the decomposition of the line current using spectral decomposition architecture using filter bank units. The concept of subband decomposition using filter banks is been used in this work. The spectral representation coefficients could be used in as signal reference for estimation of variation and then can be passed to advance learning approaches to make appropriate decisions. The use of ANNs (Artificial Neural Networks) for plant identification and control is gaining interest [5], [6]. A potential advantage of the ANN is its ability to handle the nonlinear mapping of the input–output space. The output of the proposed spectral-ANN controller is a neuron output, which may be either the quadrature or the real voltage component of the series inverter of the UPFC. The single neuron output will be either a function of the change in real power or change in the bus voltage or reactive power. This provides a nonlinear FACTS controller, which can significantly improve the transient performance of the power system.

Power Flow Controlling

The UPFC by means of series voltage injection is able to control the transmission line voltage, impedance, and the real and reactive power flow in the line. The series inverter provides the main function of the UPFC by injecting a voltage with magnitude, which is controllable and a phase angle in series with the line. This injected voltage acts essentially as a synchronous AC voltage source. The transmission line current flows through this voltage source resulting in a reactive and

active power exchange between itself and the ac system. The active power exchanged at the AC terminal is converted into dc power, which appears at the DC link as a positive or negative real power. The basic function of shunt inverter is to generate or absorb the real power demanded by series inverter at the common DC link. The power demand by the series inverter at the DC link is converted back to AC by the shunt inverter and fed to the transmission line bus. The single line UPFC architecture is presented in figure 1.

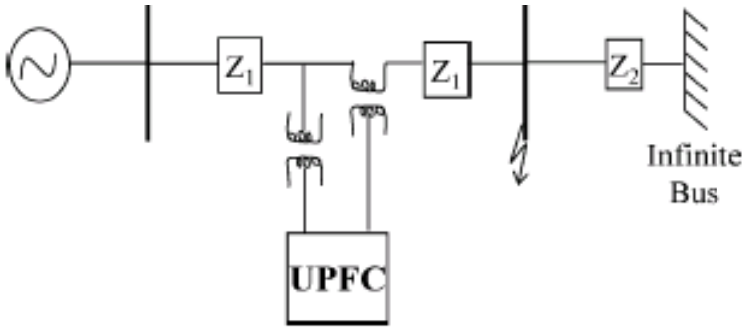

Figure 1: UPFC Architecture

In addition to this, the shunt inverter can also generate or absorb controllable reactive power if desired and thereby provides independent shunt reactive compensation for the transmission line [6],[7]. The three main control parameters of UPFC are voltage magnitude, voltage angle and shunt reactive current. The transient stability model for the shunt and series branch of a UPFC in the reference frame is given in the literature [8]. This UPFC architecture collects the transmitting current data from shunt-series insertion transformers. These currents could be processed in spectral domain for the feature estimation and disturbance detection.

System approach

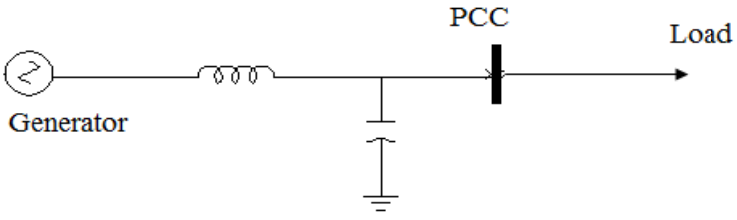

Figure 2: A Generic power flow diagram for the electrical power system

In the above conventional flow diagram series compensation is used to reduce the disturbances in current and shunt compensation is used to maintain constant DC link

voltage which is illustrated diagrammatically in figure3.

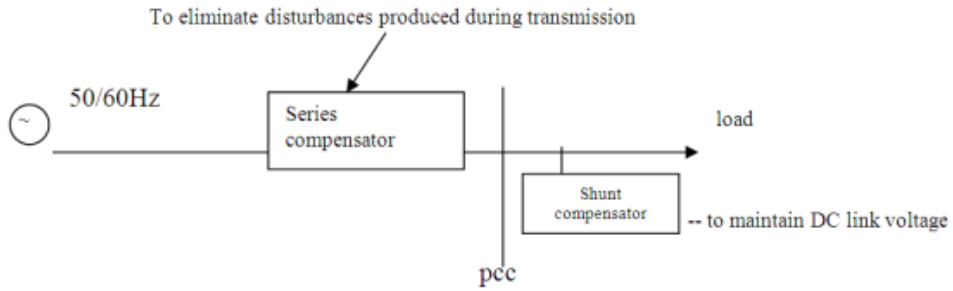

Figure 3: Conventional series and shunt compensator placement

In case of disturbances the current signal may consists of high frequency and low frequency components. The evaluation of high frequency components is easy as compared to that of low frequency components for a given band of frequencies. But ignoring low frequency components results in saturation of power transformers leading to voltage sag or swell or harmonics. Thus it is necessary to consider various ranges of spectral components of the signal instead of single band of a signal for analysis. Hence signal processing tool with the characteristics of multi resolution analysis (MRA) is deemed necessary for appropriate compensation of power quality problem.

In this paper wavelet transform is proposed due to its ability of multi level decomposition of a signal (non-stationary). The proposed approach with wavelet transformation is shown in figure 4.

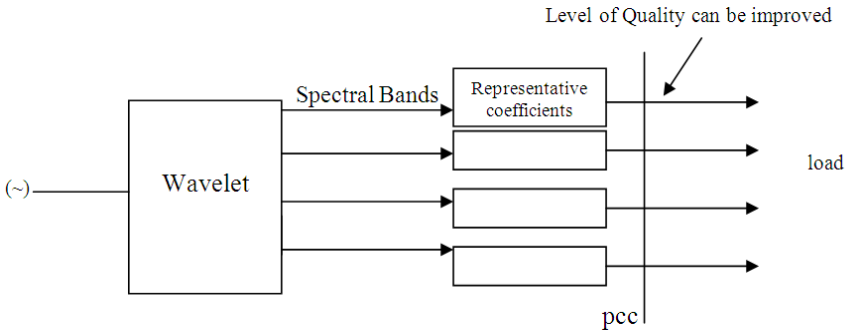

Figure 4: proposed wavelet based estimation approach

The proposed approach can further be improved by dynamic compensation which can be achieved by integrating the proposed system with a learning method such as neural network called neuro controllers. The system then gets modified as shown below.

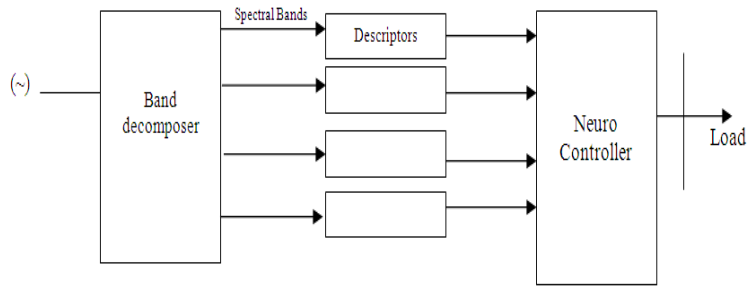

Figure 5: Proposed Hybrid Series/Shunt compensator with Wavelet-Neuro controller

Spectral-Neuro Model

The fundamental idea behind spectral analysis is to analyze the recorded current signal at different scales or resolutions, which is called multi resolution analysis. For the analysis of current signal in multi spectral domain frequency domain transformation and analysis is carried out. For the decomposition of current signal pulse into individual resolution for analysis is carried out using advanced signal transformation technique called Wavelet transformation. Wavelets are a class of functions used to localize a given signal in both space and scaling domains. Compared to Windowed Fourier analysis, a wavelet is stretched or compressed to change the size of the diagnosis window. In this way, wavelets give an approximate better analysis of the signal, while smaller and smaller wavelets explore the details of the signal. Wavelets automatically adapt to both the high frequency and the low-frequency components of a signal by different sizes of windows. Any small change in the wavelet representation produces a correspondingly small change in the measured measured signal, which means a local mistake does not influence the entire transform. With these property wavelet transform is best suited for the analysis of non-stationary current signals, which are very brief signals and with interesting components at different scales.

For the analysis of the measured current signal a wavelet function is used. The wavelet function is generated from one single function ψ, called prime wavelet, by dilations and translations defined by,

$$\psi_{a,b}(x) = \mid a \mid^{-1/2} \psi\left(\frac{x-b}{a}\right) \tag{1}$$

Where ψ satisfy the property of $\int \psi(x)\, dx = 0$.

The transformation represent any arbitrary function ‘f’ as a decomposition of the wavelet basis or write ‘f’ as an integral over ‘a’ and ‘b’ of $\psi_{a,b}$. For a given continuous current pulse, if it is defined $a = a_0^m, b = nb_0a_0^m$ with m, n € integers, and $a_0>1, b_0>0$ fixed. Then the multi-band spectral decomposition is given by,

$$f = \sum c_{m,n}(f)\psi_{m,n}\,. \tag{2}$$

for the processing of wavelet transformation a bank f filters having low pass and High pass characteristic is used. The frequency response for such filter coefficient is as illustrated in figure 6.

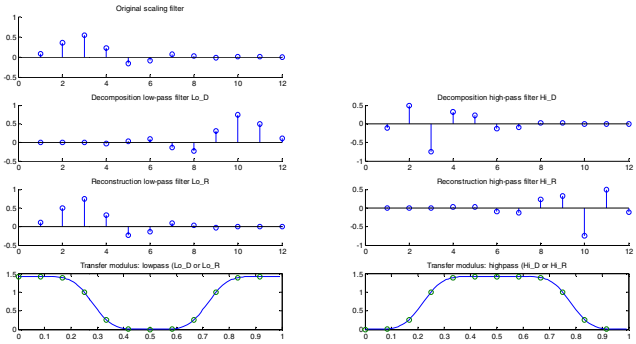

Figure 6: frequency response plot for filter coefficients used for spectral decomposition

The procedure starts with passing this signal (sequence) through a half band digital low pass filter with impulse response h [n]. Filtering a signal corresponds to the mathematical operation of convolution of the signal with the impulse response of the filter. The convolution operation in discrete time is defined by:

$$x[n] * h[n] = \sum_{k=-\infty}^{\infty} x[k] \cdot h[n-k] \tag{3}$$

A half band low pass filter removes all frequencies that are above half of the highest frequency in the signal. One way to built sub-band codification is to split the spectrum into frequency bands which consumes more processing time. Therefore it is convenient to split the given signal into two bands of spectral components such as low pass filtered and high pass filtered components. The high pass filtered components gives the smallest information where as low pass filtered components gives information regarding further minutely varying details until desired number of bands.

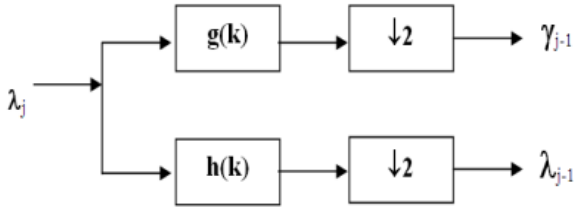

Figure 7: Implementation of one stage iterated filter bank.

The process of splitting the spectrum is graphically represented in figure 7. The advantage of this scheme is that it is necessary to design only two filters & the disadvantage is that the signal spectrum coverage is fixed. The wavelet transform is the same as that of a sub-band coding scheme using a constant-Q filter bank. The detail coefficients cD are consisting high-frequency content and the approximation coefficients cA contain the low frequency content of the signal. The actual lengths of the detail and approximation coefficient vectors are slightly more than half the length of the original signal. This has to do with the filtering process, which is implemented by convolving the signal with a filter. By observing the features obtained by discrete wavelet transform it is easy to detect, locate and classify the disturbance. A program was developed and implemented in MATLAB environment using the following steps.

Step 1: Obtain the wavelet coefficients of the pure sinusoidal signal.
Step 2: Calculate the square of the wavelet coefficients obtained in the above step.
Step 3: Calculate the signal energy, in each wavelet coefficient level which is given by Parseval's theorem.
Step 4: Repeat the above procedure for distorted signal.
Step 5: Compare the total distorted signal energy to that of pure signal energy value.

The evaluated wavelet coefficients after the execution of the suggested algorithm as outlined above results are the processed by a neuro controller for the controlling of power flow for quality improvement in power system.

Neuro controlling

The ability to identify the interactions between cause and effect of a system made the neural networks more suitable for modeling and designing intelligent controllers for power systems [4], [5]. A radial basis function (RBF) neural network controller for UPFC, based on the direct adaptive control scheme has been reported to improve the transient stability performance of a power system [6]. It is known that indirect adaptive control is able to control a nonlinear system with dynamics. The main advantage of the neuro controllers over the conventional controllers is that they can adapt to the changes in system operating conditions automatically.

The block diagram of the conventional PI controllers for shunt branch and series branch of the UPFC are shown in Figure. 9 The control of series inverter can be achieved using PQ-decoupled control. Neglecting the inverter losses, the injected active power P_{inj}, reactive power Q_{inj}, output active power P_{out}, and reactive power Q_{out} are given by the following expressions.

$$P_{inj} = \frac{V(E_q - E_q \cos\delta + E_d \sin\delta)}{X} \tag{4}$$

$$Q_{inj} = \frac{VE_d \cos\delta + V_2 E_q \sin\delta - V_2 E_d + E_d^2 + E_q^2}{X} \tag{5}$$

$$P_{out} = \frac{V_2^2 \sin\delta + V_2 E_q}{X} \tag{6}$$

$$Q_{out} = \frac{2V_2E_d\cos\delta + 2V_2E_q\sin\delta + E_d^2 + E_q^2}{2X} \tag{7}$$

Where

$$\begin{aligned} V_2 &= \sqrt{E_d^2 + E_q^2} \\ E_q &= V_{inj}\sin(\theta_{inj}) \\ E_d &= V_{inj}\cos(\theta_{inj}) \end{aligned} \tag{8}$$

It can be seen from equation (3) that P_{out} is mainly affected by E_q whereas equation (4) shows that Q_{out} is affected by both E_q and E_d. In incremental form, the line active and reactive power can be expressed in terms of ΔE_q and ΔE_d as follows.

$$\Delta P_{out} = \frac{V}{X}\Delta E_q \tag{9}$$

$$\Delta Q_{out} = \frac{1}{X}(\Delta E_d V\cos\delta + \Delta E_q V\sin\delta + \Delta E_d E_{do} + \Delta E_q E_{qo}) \tag{10}$$

However, it can be assumed in practice that cosδ is close to unity and sinδ is close to zero since the phase angle between the two buses (receiving and sending ends) on a transmission line is less than 30.

Control of the shunt active and reactive current is achieved by varying the shunt inverter voltage active component E_{pd} and reactive component E_{pq}, respectively. Figure 9 shows a typical block diagram of the conventional PI controllers for the UPFC shunt branch control [8], [9]. The outputs of this control system are the modulation index k and phase shift α. The PI controllers are replaced by the neuro controllers.

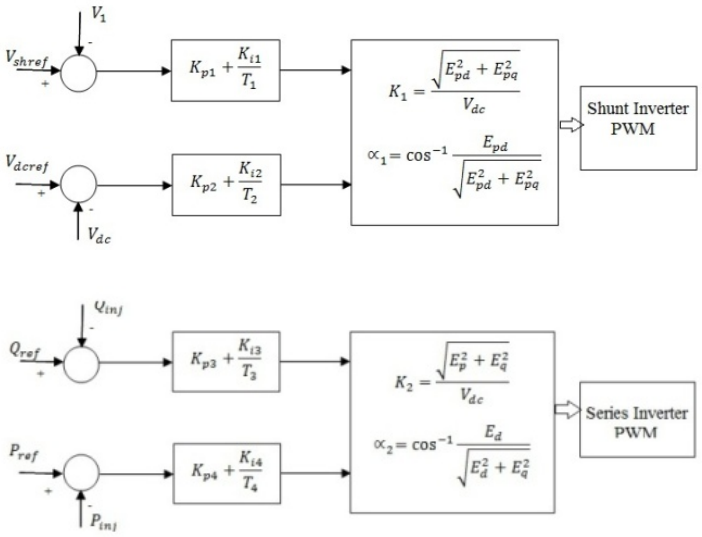

Figure 9: Shunt & series inverter control with PI controllers.

Two neuro predictor (NI), one for the series inverter and the other for the shunt inverter are used to identify the hybrid dynamics of the UPFC and the power system. These networks dynamically identify the controlling parameters of UPFC ΔE_{pd}, $\Delta E_{pq,}\Delta E_{p,}$ ΔE_q which are the outputs of the controllers. The NPs are developed using the series-parallel Nonlinear Auto-Regressive Moving Average (NARMA) model [4]. The two neuropredictor are continually online trained simultaneously to provide dynamic models at all times. The training of NPs takes place in two phases, namely, a pre-control phase and a post control phase [5].

The series branch neuro identifier is a three-layer feed forward neural network with 13 inputs, a single hidden layer with 15 sigmoid neurons, and two outputs. There are two different types of training that are carried out for NP, namely, the forced training and the natural training. During forced training, the dynamics of the system are tracked by applying perturbations which are fed to the system. During natural training the inputs to the system at are the controller outputs, where the controller can be a conventional PI controller or a Neuro controller (NC). The neural controllers design used is same as explained in [4].

The algorithm used for the modeling of the WNC is as outlined below,

STEP 1: The system output signals are sampled and time delayed by one, two and three sample periods.

STEP 2: The sampled signals from step 1 are input to the NC which then calculates the signals ΔE_d and ΔE_q which are used to train the NP as well as to control the system.

STEP 3: These control signals are time delayed by one, two and three sample periods and together with the signals from step 1 are inputs to the NP.

STEP 4: The outputs $(P_{err}(t)$ and $Q_{err}(t))$ and the outputs of NP $P_{err}(t+1)$ and $Q_{err}(t+1)$ are subtracted to produce error signals which are back propagated to update weights of NP.

STEP 5: In the post-control training of NC, the output of the NP $P_{err}\ (t+1)$ and $Q_{err}\ (t+1)$, and the desired response predictor $(P_{err}\ (t+1)$ and $Q_{err}\ (t+1))$ are subtracted to produce a second error signal. The error signal is back propagated through the NP and the derivatives are obtained with changing the weights of the neuroidentifier.

STEP 6: The back-propagated signal is subtracted from the output signal of the NC to produce an error signal.

STEP 7: This error signal is then used to update the weights in the NC, using the back propagation algorithm. This causes the NC to change its output in a way, which drives all the error signals to zero.

STEP 8 : New control signals are calculated ΔE_d and ΔE_q, using the updated weights in step 7 and are then applied at time $(t+1)$.

STEP 9: These steps (1 to 8) are repeated for subsequent time periods.

Result Observations

For the evaluation of the developed controlling system a 13-Bus IEEE bus structures

is used with the variation in line parameters. To evaluate the process of power flow controlling carried out the process is as outlined below,

IEEE-13 Bus system:
Line diagram

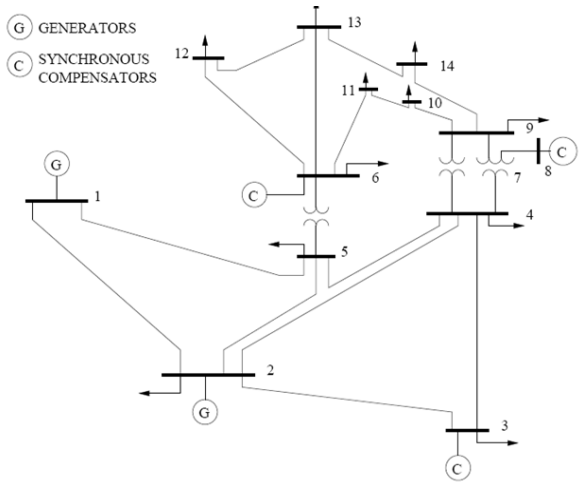

Figure 10: IEEE-13 Bus system line diagram

Figure illustrates the line diagram for a 13 Bus distributed network considered for simulation perspective.

Line Data parameter

From Bus	To Bus	Resistance (p.u.)	Reactance (p.u)	Line charging (p.u.)	tap ratio
1	2	0.01938	0.05917	0.0528	1
1	5	0.05403	0.22304	0.0492	1
2	3	0.04699	0.19797	0.0438	1
2	4	0.05811	0.17632	0.0374	1
2	5	0.05695	0.17388	0.034	1
3	4	0.06701	0.17103	0.0346	1
4	5	0.01335	0.04211	0.0128	1
4	7	0.00	0.20912	0.00	0.978
4	9	0.00	0.55618	0.00	0.969
5	6	0.00	0.25202	0.00	0.932
6	11	0.09498	0.1989	0.00	1
6	12	0.12291	0.25581	0.00	1
6	13	0.06615	0.13027	0.00	1
7	8	0.00	0.17615	0.00	1
7	9	0.00	0.11001	0.00	1
9	10	0.03181	0.08450	0.00	1
9	14	0.12711	0.27038	0.00	1
10	11	0.08205	0.19207	0.00	1
12	13	0.22092	0.19988	0.00	1
13	14	0.17093	0.34802	0.00	1

A load flow analysis is carried out using Newton raphson method on the 13 Bus systems and the Reactive power loss on the transmission line is computed. The analysis is carried out with the placement of controlling device on bus 1-2, 1-5 and 2-3 lines. The reactive power loss is observed to be reduced in case of WNC-UPFC as compared to conventional approach.

Load flow analysis

From-Bus	To-Bus	without-UPFC	Neuro-UPFC	WNC-UPFC	Xl	Xc	%compensation
1.0000	2.0000	12.9630	5.7350	4.8280	0.0592	0.0292	49.3662
1.0000	5.0000	11.6430	7.1320	6.7740	0.2230	0.1092	48.9778
2.0000	3.0000	9.5990	6.8760	6.6640	0.1980	0.0638	32.2120
2.0000	4.0000	5.0870	3.7500	2.7500	0.1763	0.0550	31.2046
2.0000	5.0000	2.8210	2.1810	1.1810	0.1739	0.0439	25.2358
3.0000	4.0000	0.9630	0.1910	0.1910	0.1710	0.0414	24.2238
4.0000	5.0000	1.4940	1.4470	1.4170	0.0421	0.0089	21.1589
4.0000	7.0000	1.6310	1.6830	1.6520	0.2091	0.0420	20.0937
4.0000	9.0000	1.2770	1.2560	1.2810	0.5562	0.1108	19.9180
5.0000	6.0000	5.1520	6.2470	5.2470	0.2520	0.0497	19.7286
6.0000	11.0000	0.2650	0.2690	0.2690	0.1989	0.0382	19.2056
6.0000	12.0000	0.1670	0.1670	0.1680	0.2558	0.0491	19.1978
6.0000	13.0000	0.4940	0.4860	0.4960	0.1303	0.0245	18.7841
7.0000	8.0000	1.1110	1.1460	1.1460	0.1762	0.0255	14.4479
7.0000	9.0000	1.0500	1.0730	1.0500	0.1100	0.0155	14.0987
9.0000	10.0000	0.0200	0.0280	0.0200	0.0845	0.0113	13.3728
9.0000	14.0000	0.2010	0.2140	0.2020	0.2704	0.0354	13.0853
10.0000	11.0000	0.1290	0.1340	0.1330	0.1921	0.0037	1.9108
12.0000	13.0000	0.0100	0.0100	0.0100	0.1999	0.0036	1.7911
13.0000	14.0000	0.2180	0.2220	0.2220	0.3480	0.0062	1.7873

The measured 3-phase line currents are derived from the network as shown figure below, 3-phase Line current:

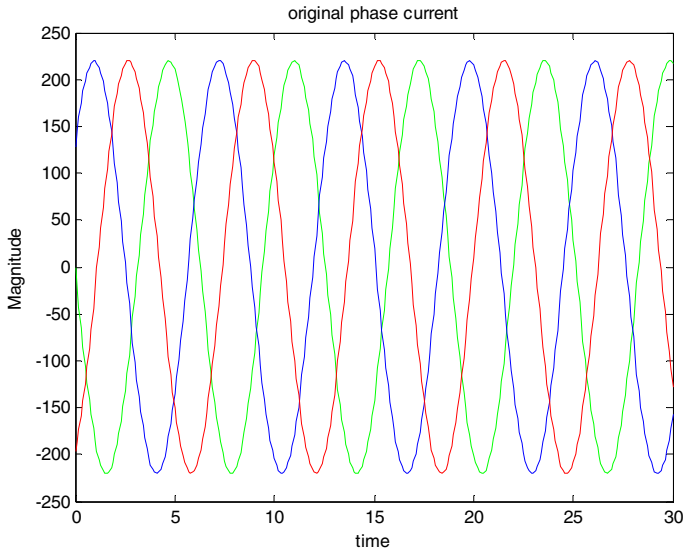

Figure 11: Original disturbance free 3-phase current

Spectral analysis of the measured current pulse

The measured 3 phase line currents are processed for spectral analysis using dynamic wavelet coefficients. Two approach of wavelet coefficient are used for the processing namely complex morlet wavelet and frequency B-spline transform. The suitability of these filters for spectral analysis is observed to be effective due to its adaptive nature of analysis and synthesis filtration. The frequency characteristic for used filter coefficient is as shown below,

Wave-coefficient (Complex Morlet)

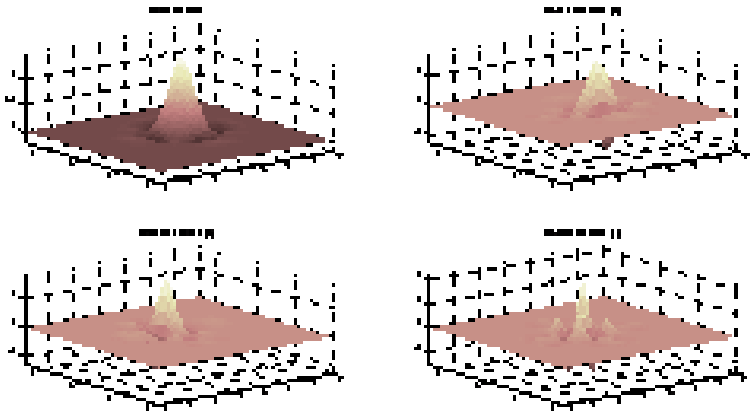

Figure 12: frequency characteristic of morlet wavelet coefficient used for spectral analysis

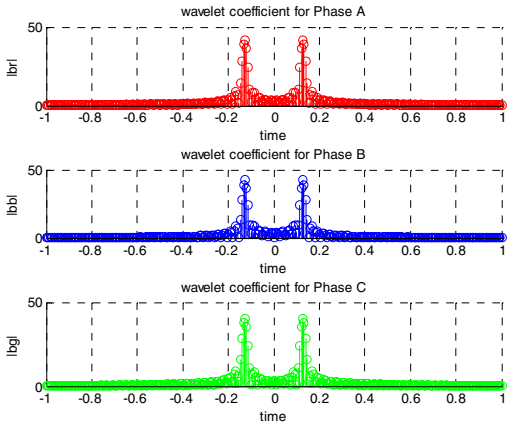

Figure 13: the coefficient density per phase on the application of wavelet transform

The per phase current is processed for spectral analysis using the stated filter coefficient. the magnitude of the three line currents are observed ot be at a range of 50dB magnitude. The disturbance free coefficients are hence observed to give a

reference margin of 50dB spectral content which is set as a reference in coefficient mapping for selecting coefficients. A similar transformation is also carried out using requency B-spline transformation as they are very effective in processing any continuous signal with frequency variation wrt. time. The coefficient characteristic for such filter could be observed below,

Wave-coefficient (Frequency B-Spline)

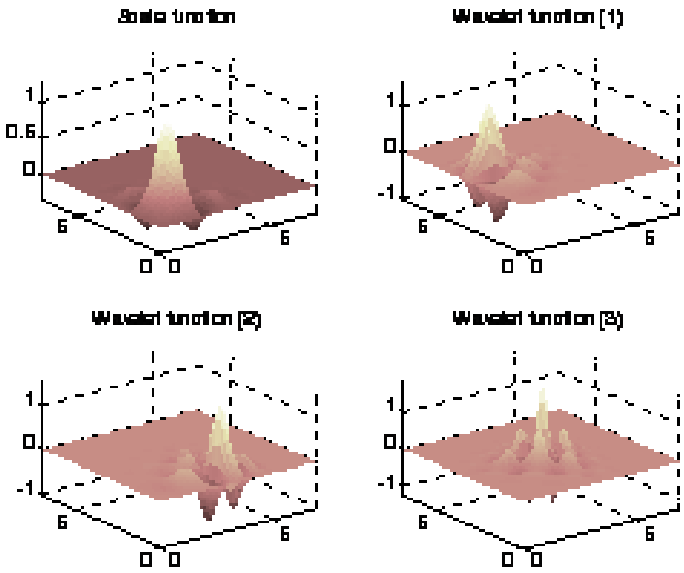

Figure 14: response characteristic for frequency B-Spline coefficient used for transformation

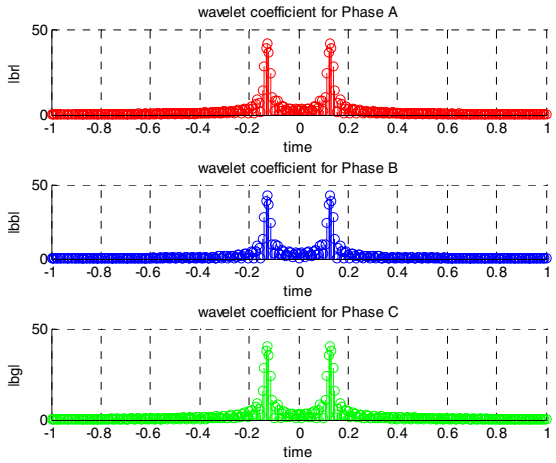

Figure 15: Spectral coefficients derived from frequency B-spline transformation

Spectrum analysis

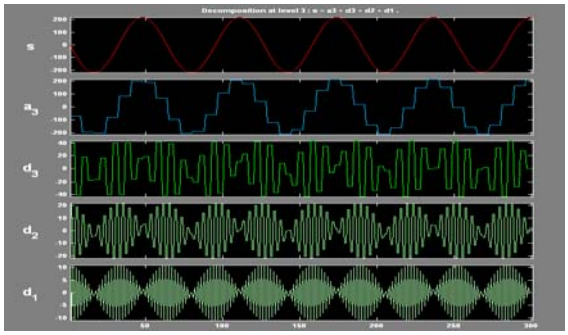

Figure 16: Spectral coefficient of first four bands for a non effected current pulse

The spectral analysis for a single phase non effected current pulse is as shown in figure above. It is clearly observed that the current pulse have very dominant coefficient density at lower frequency region as compared to higher frequency band. The coefficient domination at the particular frequency band helps in extracting the required coefficient suppressing the other frequency content than the fundamental frequency.

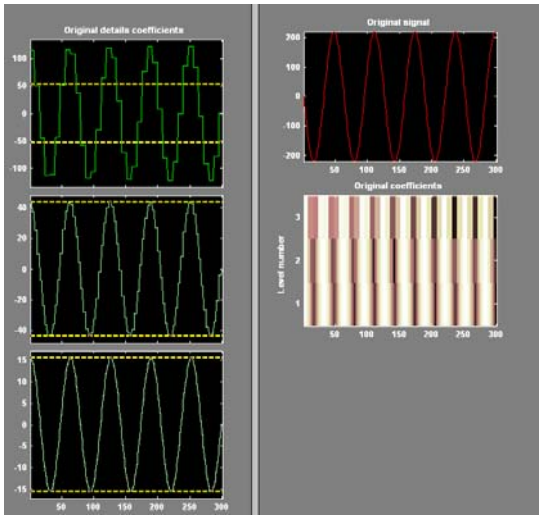

Figure 17: the processed detail coefficient for compression and disturbance removal approach using spectral analysis

Figure above illustrates the coefficients extracted after compression and decomposition of the current pulse. The coefficients are observed to be effectively reducing the coefficient counts and improve the current pulse quality by removing additional coefficients.

Spectral coefficient Density for 3-phase Complex Morlet wave transformation

phase	$\|D1\|^2$	$\|D2\|^2$	$\|D3\|^2$
R	48.3	47.4	48.5
Y	48.5	48.3	47.97
B	46.7	46.33	46.12

Frequency B-Spline wave transformation

phase	$\|D1\|^2$	$\|D2\|^2$	$\|D3\|^2$
R	49.11	49.44	49.76
Y	48.7	48.74	48.97
B	47.8	47.43	47.52

The density of magnitude for the three phase current and its detail coefficients are as presented in above table. These figures are taken as reference for the extraction of actual current pulse from the measured one. For the evaluation of the suggested approach the measured current pulse is applied with a fault effect and is processed for its effect removal. For the evaluation of the suggested approach, a three-phase line distortion due to line effects of a 100 ms duration is created at the middle of the transmission line connecting bus-1 and bus-2.

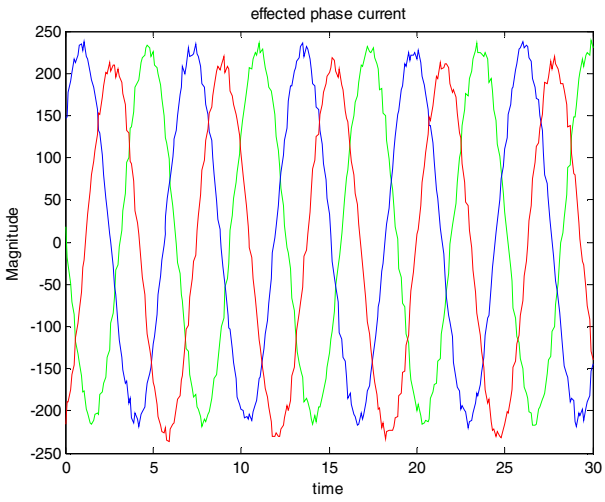

Figure 18: measured effective current pulse after the fault effect

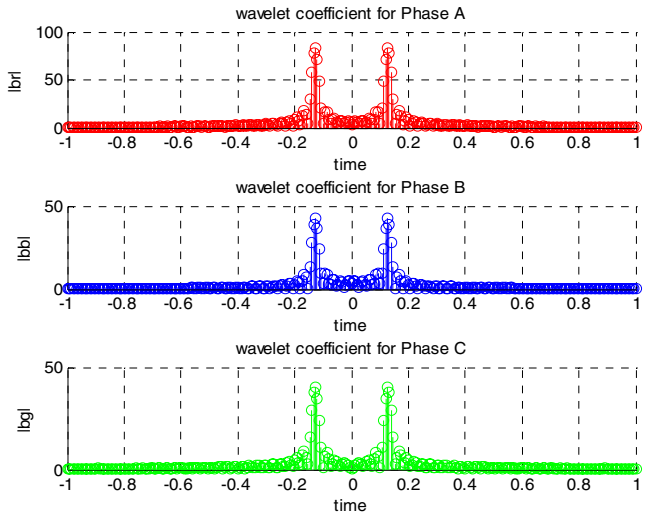

Figure 19: coefficient density plot for the three phase spectral coefficients

Figure illustrates the effective coefficient density observed after fault effect. it could be clearly observed that the coefficients under fault condition is dominantly increased to about 80 units in faulty condition as compared to a healthy condition.

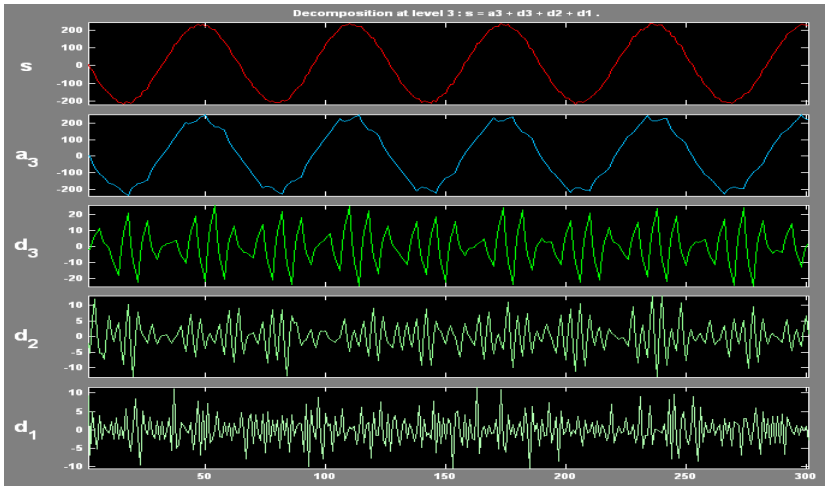

Figure 20: spectral coefficient analysis for the measured fault current

Figure illustrates the spectral coefficient analysis under fault condition. the analysis clearly illustrates the density of variation in detail coefficient magnitudes due to variation in the current magnitude.

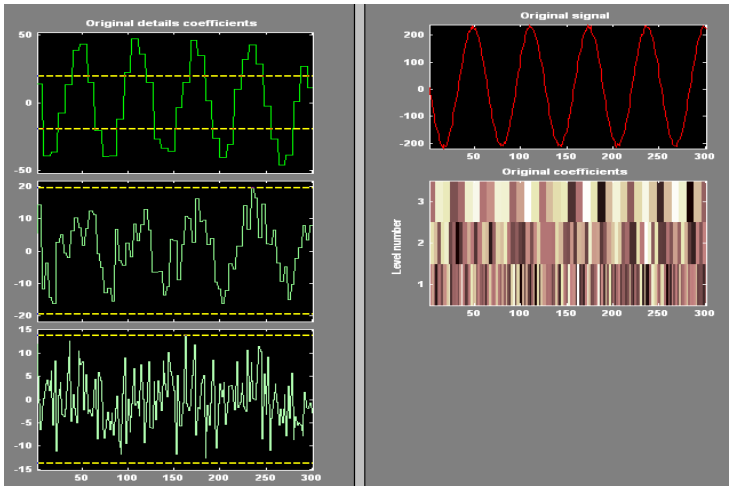

Figure 21: decomposed and extracted noise signal from the processed signal

The signal after removal of additional disturbances could be observed in above figure. The process clearly illustrates that the spectral analysis of the current pulse remove the undesired coefficient as well reduces the coefficient counts for processing. This improves the efficiency of neuro controller to make the decision faster and accurately.

Neuro controlling operation

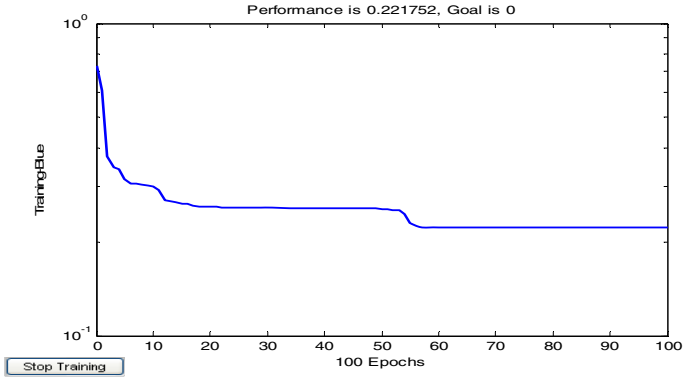

Figure 22: Learning error for the designed neuro controller

1. The performance of the conventional PI controller, MLNN controller and single neuron RBFNN controller in damping the local mode of oscillations of the generators are presented in figure below. In this case the control of series voltage source is taken. The performance of proposed WNC-UPFC is quite promising in comparison to the PI, MLNN controller and single neuron-RBF controller.

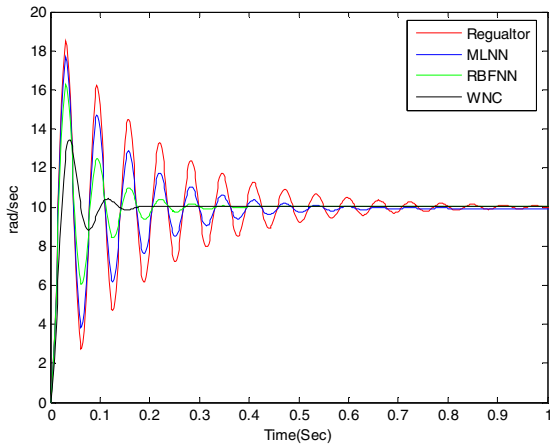

Figure 23: transient response of local mode of oscillation

2. The operating condition of the network is then changed to p=0.433,Q=0.136, and the fault of case-1 is created to test the robustness of the proposed WNC controller compared to single neuron RBFNN controller with change in operating condition. the made observation clearly depicts its robustness for operating condition changes.

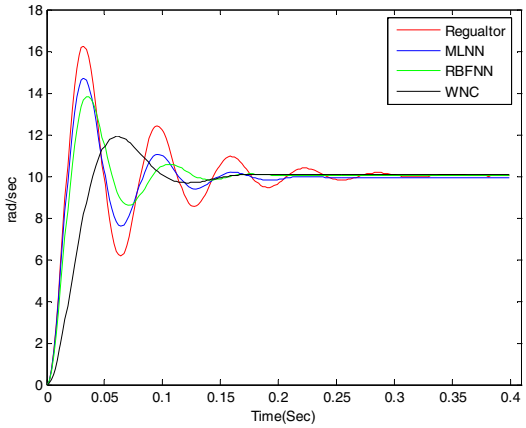

Figure 24 : transient response of local mode of oscillation

3. To test the robustness of the WNC controller to fault location a three-phase fault of 100 ms duration is created at the middle of one of the transmission line with the loading of generators same as case-1. The performances of the controller for damping modal oscillations are presented in Figs.below. The superiority of WNC controller for such a system is compared with the single neuron RBFNN controller.

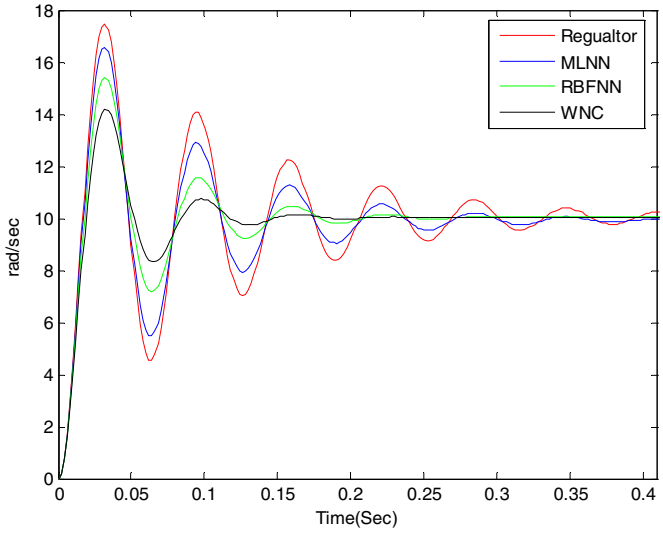

Figure 25: transient response of local mode of oscillation

Table: system convergence time under different conditions of UPFC model

Neuro Model	Hidden Nodes	Wave-function	converging Time
BP-FF	6	symlet	12 sec
BP-FF	15	symlet	19 sec
BP-FF	30	Symlet	21 sec
RBF	6	Biorthogonal-2.2	11 sec
RBF	15	Biorthogonal-2.2	17 sec
RBF	30	Biorthogonal-2.2	19 sec

The observation developed for various neuro models' using both spectral transformations is carried out. The numbers of intermediate neurons are varied with transformation approach. The convergence time taken to make a decision for such a system is outlined in the table given.

Conclusion

In this paper, the design of two continually on-line trained neuro-controllers with wavelet feature is presented. This method provides adaptive nonlinear indirect control of the series and shunt inverters of UPFC. It has been shown here that the two separate wavelet based neuro controllers are able to identify successfully the hybrid dynamics of UPFC and power system. The results prove that wavelet trained neuro-controller can effectively damp out the oscillations and increases the voltage stability margin than the conventional controller.

References

[1] R. M. Mathur & R. K. Varma, Thyristor-Based Facts Controllers for Electrical Transmission Systems. New York: IEEE Press/Wiley, 2002.

[2] L. Chunlei, S. Hongbo, and D. C. Yu, "A novel method of power flow analysis with unified power flowcontroller (UPFC)," in Proc. IEEE-PES Winter Meeting, vol. 4, 2000, pp. 2800–2805.

[3] N. G. Hingorani and L. Gyugyi, Understanding FACTS Concepts and Technology of Flexible AC Transmission Systems. New York: IEEE Press, 2000.

[4] G. K. Venayagamoorthy and R. G. Harley, "Two separate continually online-trained neurocontrollers for excitation and turbine control of a turbo generator," IEEE Trans. Ind. Appl., vol. 38, no. 3, pp. 887–893,May/Jun. 2002.

[5] "A continually online trained neurocontroller for excitation and turbine control of a turbo generator," IEEE Trans. Energy Convers., vol. 16, no. 3, pp. 261–269, Sep. 2001.

[6] P. K. Dash, S. Mishra, and G. Panda, "A radial basis function neural network controller for UPFC," IEEE Trans. Power Syst., vol. 15, no. 4, pp. 1293-1299, Nov. 2000.

[7] R. P. Kalyani and G. K. Venayagamoorthy, "A continually online trained neurocontroller for the series branch control of the UPFC," in Proc. INNS-IEEE Int. Joint Conf. Neural Networks, vol. 4, Jul. 2003, pp. 2982–2987.

[8] L. Y. Dong, L. Zhang, and M. L. Crow, "A new control strategy for the unified power flow controller," in Proc. IEEE-PES Winter Meeting, vol. 1, 2002, pp. 562–566.

[9] P. M. Anderson and A. A. Fouad, Power System Control and Stability. New York: IEEE Press, 1994.

[10] B. A. Renz, A. Keri, A. S. Mehraban, C. Schauder, E. Stacey, L. Kovalsky, L. Gyugyi, and A. Edris, "AEP unified power flow controller performance," IEEE Trans. Power Del., vol. 14, no. 4, pp. 1374–1381, Oct. 1999.

[11] A. Edris, "FACTS technology development: An update," IEEE Power Eng. Rev., vol. 20, no. 3, pp. 4–9, Mar. 2000.

[12] S.Wei and X. Zheng, "Per unit model of UPFC and its optimal control," in Proc. IEEE-PES Winter Meeting, vol. 3, 2000, pp. 1105–1108.

[13] T. T. Ma and K. L. Lo, "Nonlinear power system damping control strategies for the unified power flow controller (UPFC)," in Proc. PowerCon'00, vol. 2, 2000, pp. 673–678.

[14] G. K. Venayagamoorthy, R. G. Harley, and D. C. Wunsch, "Dual heuristic programming excitation neuro control for generators in a multi machine power system," IEEE Trans. Ind. Appl., vol. 39, no. 2, pp. 382–394, Mar./Apr. 2003.

[15] Robertson, D.C., Camps, O. I., Mayer, J.S., Wavelets and electromagnetic power system transients , IEEE Transactions on Power Delivery, Vol. 11, No. 2, April 1996, p.924-930.

[16] Gaouda. A. M., Salama. M. M. A., Sultan M. R., Chikhani. A.Y., Power quality detection and classification using wavelet-multi resolution signal

decomposition, IEEE Transactions on Power Delivery, Vol.14, No. 4, October 1999, p. 1469-1476.

[17] Burrus, C. S., Gopinath, A. R., Wickerhauser, M. V., Wavelets and time frequency analysis , Proceedings of the IEEE, vol. 84, No. 4, April 1996, pp. 523-540.